Chem. Chem. Technol., 2025,
Vol. 20, No. 1, pp. 037–052

Chemistry

PHYSICO-CHEMICAL STUDY ON THE MECHANISM OF INTERACTION BETWEEN DIVALENT AND TRIVALENT IRON DOUBLE OXIDE NANOPARTICLES WITH FIBRILLAR PROTEIN-GELATIN

Iryna Tsykhanovska[1], Tetiana Lazarieva[1], Olexandr Alexandrov[1], Mykola Riabchykov[2], Alla Koval[3], Oksana Bryzytska[4,✉]

[1] V.N. Karazin Kharkiv National University, 4 Svobody Sq., Kharkiv 61022, Ukraine
[2] Lutsk National Technical University, 75 Lvivska St., Lutsk 43018, Ukraine
[3] National University of Pharmacy, 53 H. Skovorody St., Kharkiv 61002, Ukraine
[4] PIHE "Kharkiv International Medical University", 38 Molochna St., Kharkiv 61001, Ukraine
✉ *oksanabrizi69@gmail.com*

https:// doi.org 10.23939/chcht20.01.037

Abstract. The study investigates the interaction mechanism between ferrum(II, III) oxide (Fe_3O_4) nanoparticles and the fibrillar protein gelatin (Gel) using a set of physicochemical methods. For the first time, it was established that the formation of a stable intermolecular complex is due to the **amphiphilic and clusterophilic properties** of Fe_3O_4 nanoparticles, their **ability to polarize**, **electrostatic interactions**, and **the formation of supramolecular structures**. **Absorption in the region of 260 nm (UV-Vis spectroscopy)** indicates the formation of **plasmon resonance** in the $NPFe_3O_4$/Gel system. **Dynamic Light Scattering (DLS)** revealed an average hydrodynamic particle diameter of approximately **79.0 nm**, which is consistent with **X-ray diffraction (XRD)** data and confirms the **chemisorption of the Gel protein** on the surface of Fe_3O_4 nanoparticles.
The work has scientific novelty in understanding the specifics of **biopolymer binding with metal oxide nanostructures**.

Keywords: Fe_3O_4 nanoparticles, Gel, chemisorption, nano associates.

1. Introduction

In modern chemical science, there is a growing interest in the use of nanostructured materials, particularly metal and metal oxide nanoparticles, for modifying the functional and technological properties of biopolymeric systems.[1-3] Products of the agro-industrial complex typically have polyphase heterogeneous structures, whose stability is determined by the interaction of proteins, polysaccharides**,** lipids, and other components.[4-7] Proteins play a key role in structure formation, determine the textural characteristics of the final product, and exhibit stabilizing effects.[8-10] A promising direction is the use of iron oxide (Fe_3O_4) nanoparticles, which are capable of forming new supramolecular structures with biopolymers, particularly with proteins such as gelatin — a fibrillar protein with pronounced gelling properties.[1,12] Such systems may enhance gel and foam formation, increase water and fat-binding capacity of protein systems, and ensure their structural stability.[13,14]

Despite numerous studies, the mechanisms of Fe_3O_4 interaction with proteins remain insufficiently understood, which complicates the rational design of stable nanohybrid systems.[15-17] As the processes of structure formation and dispersion stabilization via Fe_3O_4 nanoparticles and their interaction with biopolymer molecules, particularly proteins, are not fully explored or theoretically grounded, this study presents an investigation focused on identifying the nature of Fe_3O_4 nanoparticle interactions with the fibrillar protein gelatin (Gel). Establishing the interaction mechanism between Fe_3O_4 and proteins will enable the development of new, effective methods for creating nanoassociates.

The relevance of this study is driven by the need for both theoretical justification and experimental confirmation of such mechanisms at the macro- and micro-levels. The aim of the study is to clarify the

physicochemical aspects of the interaction between Fe_3O_4 nanoparticles and fibrillar gelatin protein using physicochemical research methods. Objectives include investigating the electrostatic and molecular mechanisms of stable complex formation, determining the structural and dimensional characteristics of the hybrid system, and identifying the influence of nanoparticles on the spectral and dispersion properties of the protein.

2. Experimental

2.1. Materials

Research subjects: Nanoparticles of divalent and trivalent iron oxide (Fe_3O_4) and fibrillar protein gelatin (Gel) were selected for the study, since these substances have the most significant potential for improving the functional and technological properties of polyphase systems:

– sample 1 – ultrafine Fe_3O_4 powder ($NPFe_3O_4$) with a particle size of (70±5) nm (scanning electron microscope)[17] and ζ-potential in aqueous suspensions of (35±5) mV.[11] It was obtained by the method improved by the authors, based on the reaction of chemical coprecipitation of iron (II) and (III) salts in an alkaline medium.[10,17] The precipitate was washed with distilled water and dried at 100 ºC for 60 min. The dark brown $NPFe_3O_4$ powder is a mixture of iron oxides FeO and Fe_2O_3 with an iron content of > 90%. The synthesized nanoparticles are resistant to external factors and oxidation;[15,17]

– sample 2 – Gel, gelatin-A (pork skin extract, bloom=300, GELITA TM company, Germany);

– sample 3 – $NPFe_3O_4$, modified with gelatin, namely the $NPFe_3O_4$+Gel system. The modification of the $NPFe_3O_4$ surface with gelatin was performed as follows: an aqueous solution of gelatin (0.8%, 10 mL) was added dropwise to the dispersion of nanoparticles (~ 100 nm). After incubation of the obtained $NPFe_3O_4$+Gel mixture for 24 h at 38–40°C, the modified particles were collected using a magnetic collector and dried in a vacuum for further characterization using FTIR, XRD, EDX, UV-Visible, and TGA.

– sample 4 – 3.0% aq Gel solution was prepared by hydrating the calculated amount of commercial gelatin powder with deionized water at a temperature of 50°C for ~15 min;

– samples 5, 6, 7 –Gel+ $NPFe_3O_4$ colloidal solutions, which were obtained by introducing $NPFe_3O_4$ in an amount of 1.0, 1.5, 2.0, respectively, in 3.0% gelatin-Gel solution at a temperature of 45–50°C with constant stirring n=(2.0–2.2) s^{-1} for 8–10 min, followed by holding for 5–7 min;

– samples 8, 9, 10 – amino acids with a purity of >99%: α-glycine, Gly (>99%), L-proline, Pro (>99%), L-hydroxyproline, Hyp (>99%) respectively, purchased from Sigma-Aldrich, Germany.

2.2. Methods of Analysis

2.2.1. Fourier transform infrared spectroscopy (FTIR)

The vibration spectra of experimental samples (1–3) were obtained by the method of IR-Fourier spectroscopy on an infrared spectrometer with Fourier transform Tensor 37 (Bruker Optics, Germany), controlled by the OPUS software package with standard calibration capabilities in the frequency range 4000–400 cm^{-1} in the absorption format. IR-Fourier spectra were recorded in KBr tablets.[4,10,18]

2.2.2. X-ray photoelectron spectroscopy (XPS)

XPS spectra of the experimental samples (1, 2, 6, and 7) were obtained using an Axis Ultra DLD XPS electron spectrometer (Kratos Analytical Ltd., UA), using a monochromatic Al Kα source (1486.69 eV), a hemispherical analyzer with an electrostatic lens system, charge neutralization, delay line, and detector (DLD). During the analysis, the experiments were performed using an X-ray source with a power of 180 W (15 kV and 12 mA), a pressure below 10–8 mbar. The XPS survey spectra were obtained at a pass energy of 160 eV with a step of 0.25 eV and a dwell time of 300 ms per data point at a constant take-off angle of 90°. High-resolution C, O, and N spectra were obtained at a pass energy of 20 eV with a step of 0.1 eV, with an exposure time of 300–1000 ms per data point. Peak fitting of the measured high-resolution spectra was performed by CasaXPS software using a Shirley background and Gaussian/Lorentzian line shapes (70%/30%) without fixing the peak parameters (binding energy (BE), full width at half maximum (FWHM), and area/intensity). The photoelectron lines' binding energies (BE) were determined with an accuracy of ±0.1 eV. The BE scale was referenced to the C 1s component of aliphatic carbon, set to 285.0 eV.[19–24]

2.2.3. X-ray diffraction spectroscopy (XRD)

X-ray diffraction (XRD) patterns of the studied samples (1–3) were obtained using a Bruker D8 Advance diffractometer (Bruker, Germany) equipped with a copper pole operating at 40 kV and 40 mA, generating Cu Kα alpha radiation with a wavelength of λ=1.5406 Å. The data

were obtained in the range 2θ=10–80° with a step of 0.05° and a scanning speed of 3°/s.[25–29] The crystallite sizes were calculated using the X-ray line broadening method using the Scherrer equation (1):

$$D \text{ ¼ } K\lambda=\beta\ Cos\theta \quad (1)$$

where K is the Scherrer constant with a value between 0.9 and 1.0 (form factor), λ is the wavelength of the X-ray radiation (1.54056 Å), β is the width at half maximum (FWHM) of the XRD peak, and θ is the Bragg angle. Any plane of the XRD peak can be used to determine the crystal size.

2.2.4. Energy-dispersive X-ray spectroscopy (EDX)

To determine the elemental composition of the studied samples (1–3), a JSM-820 (JEOL) scanning electron microscope with an EDX attachment was used. X-ray spectra were obtained by bombarding the studied samples with electrons using an acceleration voltage of 20 kV (corresponding to the characteristic spectra of Iron, Carbon, Oxygen, Nitrogen, Phosphorus, Potassium, Sodium, Calcium). The elemental composition of the studied samples was determined by analyzing the obtained characteristic X-ray spectra.[15,17,30]

2.2.5. Dynamic light scattering (DLS)

The values of the ζ-potential and hydrodynamic radius of Gel, NP Fe_3O_4 and the NP Fe_3O_4+Gel nanocomplex (mass ratio 1:1) were performed using dynamic light scattering (DLS) (Zetasizer Nano ZS, Malvern Instruments, United Kingdom) in a neutral medium: in deionized water (DI) (pH≤7) at a temperature of 296 K, with an aliquot of 1 mL.[10,15,31–33]

2.2.6. UV-Visible Spectroscopy

Initial characterization of the experimental samples (in particular, optical properties) was carried out using ultraviolet and visible (UV-Vis) spectroscopy using a UV 1650 PC-Shimazu B spectrophotometer (Shimazu, Osaka, Japan). The optical density of the solutions was measured in the range of 200–800 nm.[28,29,34–36]

2.2.7. Thermogravimetric analysis (TGA)

Thermogravimetric analysis of experimental samples (1–3) was performed using a TGA Perkin Elmer Diamond TG/DTA (US) analyzer in the temperature range from 20–900°C with a heating rate of 5°C/min and a constant flow of gaseous N_2.[17,18,27,28]

2.2.8. Transmission electron microscopy (TEM)

The size and morphology of nanoparticles in experimental samples (1 and 3) were studied using a transmission electron microscope (TEM) of ultra-high resolution JEOL JEM-2010 TEM (Japan), which operated at an accelerating voltage of 200 kV. The images obtained in planar geometry when the electron beam was incident along the hexagonal axis and perpendicular to it were processed using the program. UTHSCSA Image Tool version 3.0. Histograms were created using the IBM-SPSS software, and the graph was fitted using the Microsoft Excel program. The number of particles in the sample for determining the average values was at least 300.[17,35,37–41]

2.2.9. Viscosity and strength of nanostructured gelatin

The study of the rheological properties of experimental samples of Gel+NPFe_3O_4 aqueous solutions with different mass fractions of Fe_3O_4 (0; 1.0; 1.5; 2.0% of the solution mass) was carried out on a rotational rheometer (Physica MCR300, Anton Paar GmbH, Germany) equipped with parallel plate geometry (diameter 50 mm) and a gap of 0.8 mm between the two plates, with a change in the shear rate from 1 to 300 s^{-1}.[42,43] The strength of the test samples (4–7) was determined on a Stable Micro Systems TA.XTplusC texture analyzer (United Kingdom) according to the Blum method (Gelatin Manufacturers Institute Of America, 2014): in a cup with a diameter of (59±1) mm and a height of 85 mm, a gel-like sample was compressed by 4 mm (without disturbing the surface) using a Blum plunger (12.7 mm in diameter) located in the center of the cup, with a penetration speed of 0.5 mm/s. The maximum force (Fmax) is measured in grams and corresponds to the strength of the gel.[43]

3. Results and Discussion

3.1. Substantiation of the mechanism of interaction of Gel with Fe_3O_4 nanoparticles

3.1.1. X-ray photoelectron spectroscopy (XPS)

It was determined that the XP spectra of O (1s) in Fe_3O_4 nanoassociates (cumulative Fit (NPFe_3O_4), NPFe_3O_4+Gly, NPFe_3O_4+Pro, and NPFe_3O_4+Hyp have peaks at 529.5; 531.0; 533.4; 533.9 eV, which are due to O–H/Fe–O bonds arising due to the functionalization of the

amino acid matrix with chemically active, diphilic Fe_3O_4 nanoparticles.[15] Similar results were obtained in the study of composite materials based on Fe_3O_4 nanoparticles and triethylene glycol.[20] Fig. 1 presents the XP spectra of amino acids in the C (1s) region and their nanoassociates with $NPFe_3O_4$. The C (1s) peaks in the $NPFe_3O_4$+Gly nanoassociate at 284.2 and 288.4 eV are due to the σ(C–H)/ σ(C–N) and π(O–C=O) bonds, respectively. The C (1s) peaks at 288.8 and 292.6 eV in the $NPFe_3O_4$+Pro nanoassociate and at 290.6 and 294.4 eV in the $NPFe_3O_4$+Hyp nanoassociate are due to the σ(C–H)/ π(O–C=O) and σ(C–N) bonds, respectively, a slight shift of the peaks towards higher energy is observed both in amino acids (proline-Pro, hydroxyproline-Hyp) and in their nanoassociates with $NPFe_3O_4$. This is consistent with the literature sources and can be explained, firstly, by the influence of the NH-group of the heterocycle of the side chain "Pro" and "Hyp", which is also enhanced in "Hyp" by the OH-group. In addition, Fe_3O_4 nanoparticles, entering into electrostatic, steric, and other interactions with biomolecules, contribute to the formation of nanocompositions at the micro- and macro-levels.[17,24]

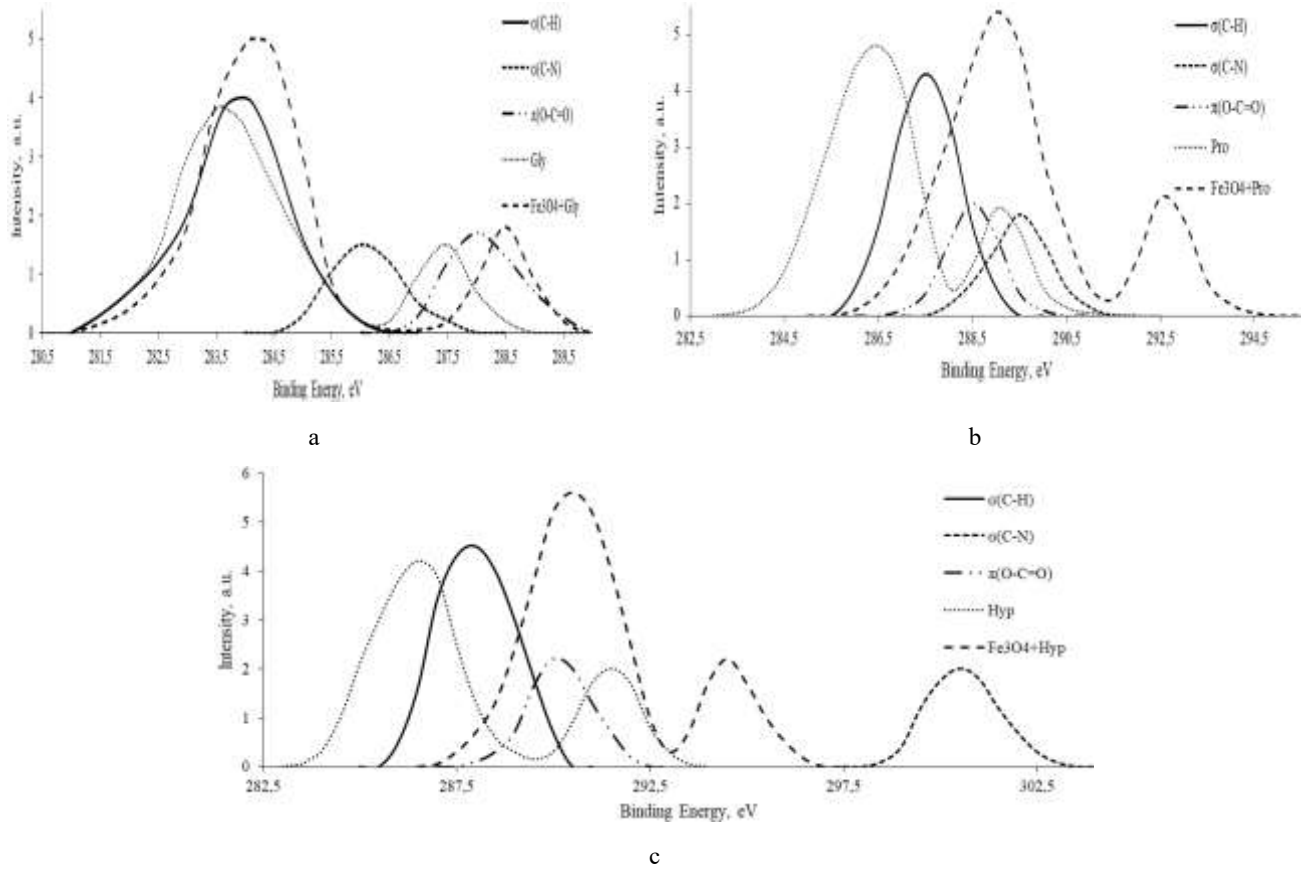

Fig.1. XP spectra in the C (1s) region of amino acids: a – glycine (Gly), b – proline (Pro), c – hydroxyproline (Hyp), and their nano-associates with $NPFe_3O_4$

3.1.2. X-ray diffraction spectroscopy (XRD)

X-ray diffraction is widely used to study nanoparticles and nanocomplex compositions, namely, the crystal structure and size of Fe_3O_4 nanoparticles and nanocomplexes based on them. The formation and stability of the $NPFe_3O_4$+Gel system were confirmed by XRD phase analysis. Fig. 2 shows the diffraction patterns of experimental samples 1, 2, and 3 ($NPFe_3O_4$, Gel, $NPFe_3O_4$+Gel, respectively).

The crystalline phases of $NPFe_3O_4$ were characterized using XRD patterns (Fig. 2). The presence of distinct Bragg peaks at 2θ=30.47°(220), 35.75°(311), 43.51°(400), 53.85°(422), 57.50°(511), 63.11°(440), and 74.54°(533) correlates with the cubic phase of Fe_3O_4 according to JCPDS Cards No. 01-089-0691 and JCPDS No. 19-0629.[20,23,24,29] This indicates that sample 1 consists of the Fe_3O_4 phase – Fe_3O_4 crystals with a spinel structure. The most intense peak corresponds to the (311) plane at an angle of 35.75° and refers to the crystallographic plane of the $NPFe_3O_4$ structure. At the same time, the average size

of sample 1 ($NPFe_3O_4$ crystals) determined using the Scherrer equation[23,31,34], is (70±5) nm.[15,23] It is known that the presence of oxygen can lead to the oxidation of Fe_3O_4 to α-hematite (α-Fe_2O_3) and γ-maghemite (γ-Fe_2O_3). However, the XRD peaks of sample 1 excluded the presence of all these undesirable substances, which is an additional confirmation of the resistance of the synthesized $NPFe_3O_4$ to oxidative processes.

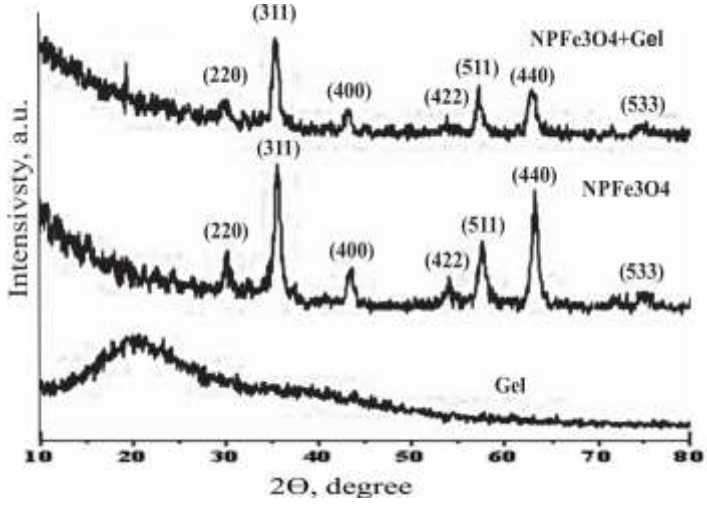

Fig.2. X-ray diffraction patterns of experimental samples:
sample 1 – $NPFe_3O_4$, sample 2 – gelatin (Gel), sample 3 –$NPFe_3O_4$+Gel nanocomplex

A broad diffraction peak at 22.35° was identified for gelatin (Gel), as shown in Fig. 2. This peak is usually attributed to the triple helical crystal structure of Gel.[23,34,39] From the experimental data (Fig. 2) it follows that the XRD diffractogram of sample 3 – the $NPFe_3O_4$+Gel nanocomplex – showed a clear crystalline nature of the nanoassociate; it displayed numerous unique peaks, in particular at (220), (311), (400), (511), and (440) which are characteristic of $NPFe_3O_4$ and Gel, and demonstrate the successful conformation of the synthesized $NPFe_3O_4$+Gel nanocomposites. At the same time, there is a tendency to decrease the intensity of the diffraction peaks in all directions of $NPFe_3O_4$ (30.47°, 35.75°, 43.51°, 53.85°, 57.50°, 63.11°, and 74.54°) and Gel (22.35°). This confirms the chemisorption of Gel on the NPFe3O4 surface and is consistent with the scientific results of other researchers.[29,33] On the other hand, Table 1 demonstrates that the crystallinity of sample 3 NPFe3O4+Gel nanocomplex increased from 63% (sample 1 $NPFe_3O_4$) to 69%.

That is, the use of Gel contributes not only to an increase in crystallinity but also to the size of $NPFe_3O_4$/Gel nanocrystallites, which is confirmed by the broadening of diffraction peaks (Fig.2). Therefore, the modification of Fe_3O_4 nanoparticles with gelatin-Gel accelerates crystallization. It increases the size of crystallites of the $NPFe_3O_4$+Gel nanocomplex, since the electrostatic interaction between the dipoles of amino and carboxy groups and dipoles of $NPFe_3O_4$ causes an increase in the molecular density of $NPFe_3O_4$+Gel nanoassociates. In addition, this contributes to the spatial rearrangement of the atoms of the system, placing each residual atom (in particular, Fe) in a more homogeneous and stable structure.[10,28,29,34,35]

Table 1. Structural properties of iron oxide nanoparticles prepared with gelatin (nanocomplex $NPFe_3O_4$+Gel) and without it ($NPFe_3O_4$)

Experimental samples	Main peak 2θ°	Crystallite size, nm	Crystallinity, %
Sample 1 – $NPFe_3O_4$	35.75	70.04	63.0
Sample 3 –$NPFe_3O_4$+Gel nanocomplex	35.76	79.44	69.0

Note: Data represent the mean ±standard deviation of three experiments (n=3).

3.1.3. Definition of ζ-potential and hydrodynamic radius

The electrokinetic potential determines the stability of dispersed systems in an aqueous environment. A higher electric charge on the surface of particles reduces their tendency to aggregate due to strong repulsive forces. The value of the ζ-potential above ±30 mV indicates a high stability of the dispersed system, in the range from ±5 mV to ±30 mV – temporary stability, and less than ±5 mV –

rapid aggregation of particles and unstable dispersion. The higher the absolute value of the ζ-potential, the lower the probability of particles to aggregate.[34,35,44,45] The effect of iron oxide nanoparticles ($NPFe_3O_4$) on the surface charge and dispersion of particles in the $NPFe_3O_4$+Gel system was studied using the ζ-potential and the dynamic light scattering method (Fig. 3).

The data in Fig. 3 demonstrate that the electrokinetic potential of the dispersed $NPFe_3O_4$+Gel system increases by (1.12–1.14) times compared to $NPFe_3O_4$ (instrument measurement accuracy: ±2% or ±0.5 mV) and by (2.14–2.16) times compared to Gel. This is consistent with the results presented in the works of other researchers.[10,34,35,44–48] At the same time, the hydrodynamic diameter of the $NPFe_3O_4$+Gel modified particles is quite small – (117.2±2.34) nm compared to other biopolymer compounds, in particular starch – (283–286) nm[35], sodium dodecyl sulfate – (197–483) nm, *etc*.[49] In addition, the data obtained for the ζ-potential and hydrodynamic diameter of the $NPFe_3O_4$+Gel system are consistent with the results of UV–VIS spectroscopy and also show that the fibrillar protein Gel prevents aggregation and growth of particles of the dispersed phase and, therefore, contributes to the preservation of colloidal stability of the dispersion. This is a factor in the stabilization of the $NPFe_3O_4$+Gel dispersed system. The interaction of Gel with $NPFe_3O_4$ causes an increase in the electrokinetic potential of the $NPFe_3O_4$+Gel system due to an increase in the surface charge and prevention of particle aggregation. The increase in the size of $NPFe_3O_4$ in solution to 77–78 nm compared to the nominal value (<d>70 nm) is due to the formation of a surface layer of H_2O molecules on the surface of $NPFe_3O_4$. In an acidic environment, $NPFe_3O_4$ actively interacts with H_2O dipoles and ionogenic groups of Gel, which contributes to the strengthening of bonds in solvate and peptide complexes.[2,15,17,50]

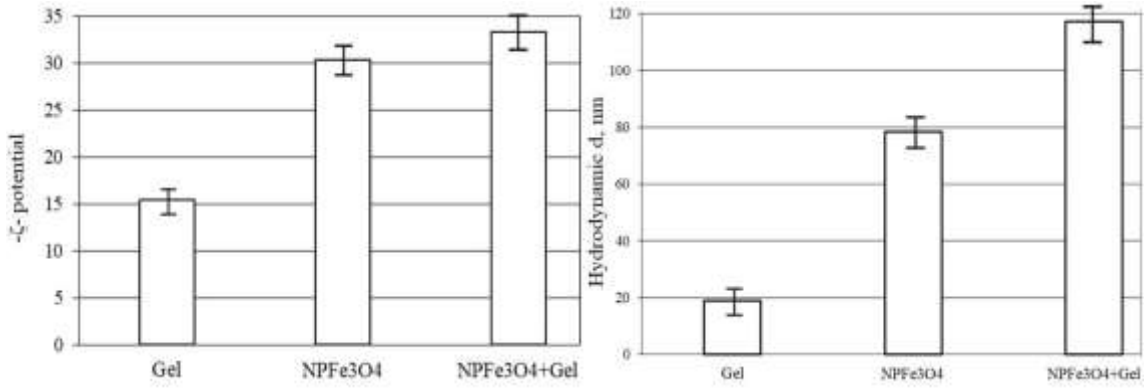

Fig. 3. ζ- potential (a) and hydrodynamic size (b) of Gel, $NPFe_3O_4$, and $NPFe_3O_4$+Gel systems in deionized water (DI) (pH ≤ 7)

The stabilization of the $NPFe_3O_4$+Gel dispersed system is effectively ensured by the formation of a double electric surface layer.[10,15,50] In the $NPFe_3O_4$+Gel nanoassociate, iron oxide nanoparticles are located at the interface of the Gel/H_2O phases, forming a monomolecular solvate layer of H_2O dipoles, which are fixed on the surface of the solid dispersed phase $NPFe_3O_4$. Gel molecules are concentrated around this layer, forming a protein shell that reduces the surface tension at the interface, contributing to an increase in the aggregative stability of the colloidal system. In addition, the Coulomb repulsive forces between like-charged particles enhance the aggregation stability of the dispersion and reduce the friction force between the particles of the dispersed phase. This provides increased stability and stability of the dispersed system, increases the electrokinetic potential, and promotes the spatial organization of colloidal particles.[3,15] Therefore, the interaction of $NPFe_3O_4$ with proteins, in particular Gel, improves the potential solubility of iron oxide nanoparticles and supports their effective use in colloidal-dispersed systems.

3.1.4. Energy-dispersive X-ray spectroscopy (EDX)

To confirm the chemisorption of gelatin-Gel on the surface of Fe_3O_4 nanoparticles, the EDX method was used, which was used to establish the chemical composition of experimental samples 1, 2, and 3: $NPFe_3O_4$, Gel, and $NPFe_3O_4$+Gel, respectively (Fig. 4).

In the X-ray spectra of the studied samples 1 (Fig. 4a) and 3 (Fig. 4 b), the values of the absorption peaks are located at about 0.8, 6.3, and 6.8 keV and are associated with the absorption of the kinetic energy of electrons of the Fe atom. In the spectra of NPFe3O4 modified with the Gel adsorption layer (Fig. 4c), there are an additional six peaks,

namely at 0.28 keV, 0.32 keV, 0.48 keV, 2.01 keV, 2.3 keV, and 3.69 keV. These absorption bands are identified as follows: C (0.28 keV), O (0.48 keV).[10,14,12,36] Moreover, the peak at 0.48 keV, characteristic of the O atom, is also present in the spectrum of pure $NPFe_3O_4$ (Fig. 6a); and the peaks at about 0.32 and 2.01 keV are associated with the absorption of kinetic energy by electrons of N and P atoms, respectively. As well as the peaks at 2.3 keV (S atom); 3.69 keV (Ca atom) - are observed in the spectra of Gel and $NPFe_3O_4$+Gel (Fig. 4 b–c).[4,10,27]

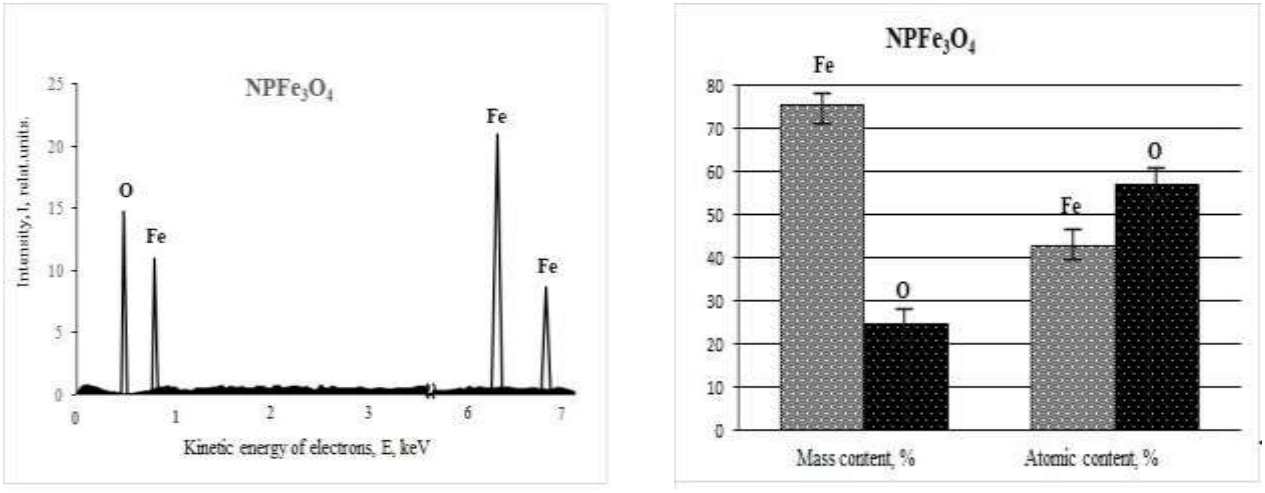

a

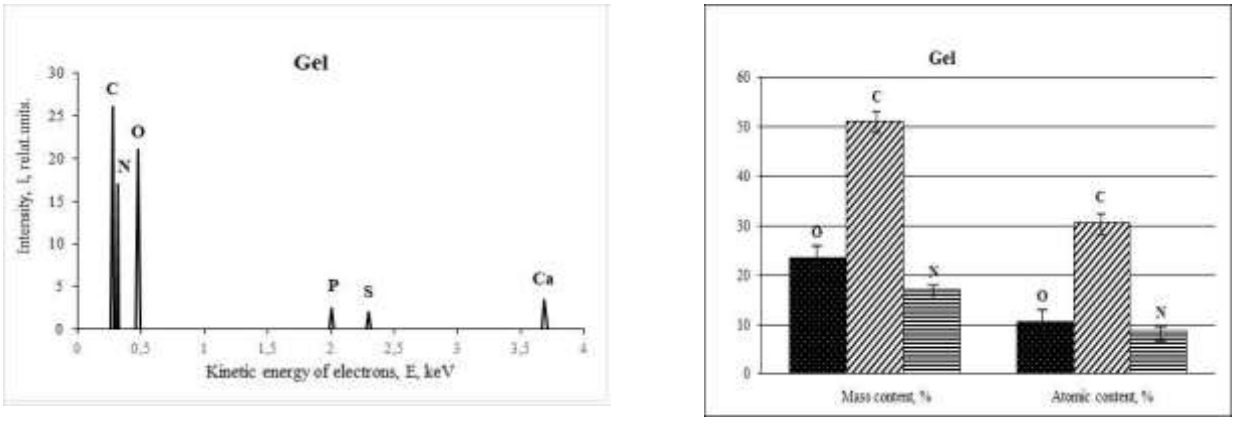

b

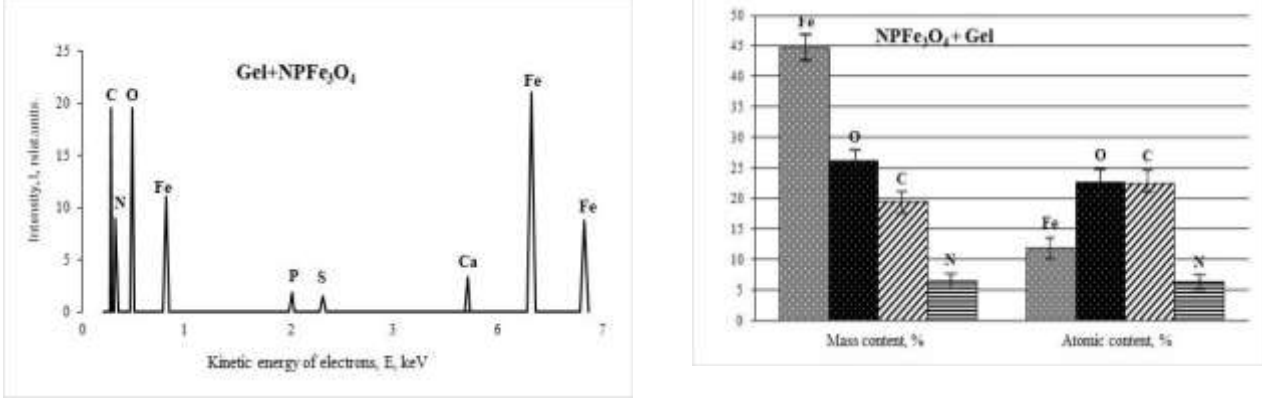

c

Fig.4. EDX spectra of test samples: a – $NPFe_3O_4$; b – Gel; c – $NPFe_3O_4$+Gel

So, from the analysis of the EDX spectra of the experimental samples, it follows that Fe, O, and C (H cannot be studied), and N, P, S, and Ca (for sample c) are the main components in the elemental composition of the nanocomplex $NPFe_3O_4$+Gel. The chemical composition of the studied samples: sample a ($NPFe_3O_4$) – Fe 75.50%; O 24.50%; sample b (Gel) – Fe 0%; O 23.5%; C 51.0%; N 17.0%; P 0.3%; S 0.1%; and Ca 0.7%; sample b ($NPFe_3O_4$+Gel) – Fe 44.8%; O 26.1%; C 19.5%; N 6.5%; P 0.12%; S 0.04%; and Ca 0.3%. Therefore, in sample b ($NPFe_3O_4$+Gel), a new chemical element (Fe) appears, absent in Gel (sample b), and five more elements (C, N, P, S, and Ca), absent in $NPFe_3O_4$ (sample a). Thus, Fe_3O_4 nanoparticles were successfully obtained (sample a), and Gel (sample b) was chemisorbed onto Fe_3O_4 nanoparticles.

3.1.5. UV-Visible Spectroscopy

The ultraviolet and visible (UV-Vis) spectra of experimental samples 1, 2, and 3: $NPFe_3O_4$, Gel, and $NPFe_3O_4$+Gel, respectively, are shown in Fig. 5. From the analysis of the data in Fig. 5, it follows that in sample 1 – $NPFe_3O_4$, a noticeable peak at 215 nm is the result of internal absorption of Fe_3O_4 nanoparticles. In this case, the mobility of electrons from the valence band to the conduction band can be determined by the equation of the energy gap (*Eg*) of Fe_3O_4 nanoparticles: $Eg=hc/\lambda$ (*c* is the speed of light, h is the Planck constant, λ is the wavelength of light); the result of the estimation of the energy of the band gap is ~4.2 eV. This confirms the identification of Fe_3O_4 nanoparticles.[37,38]

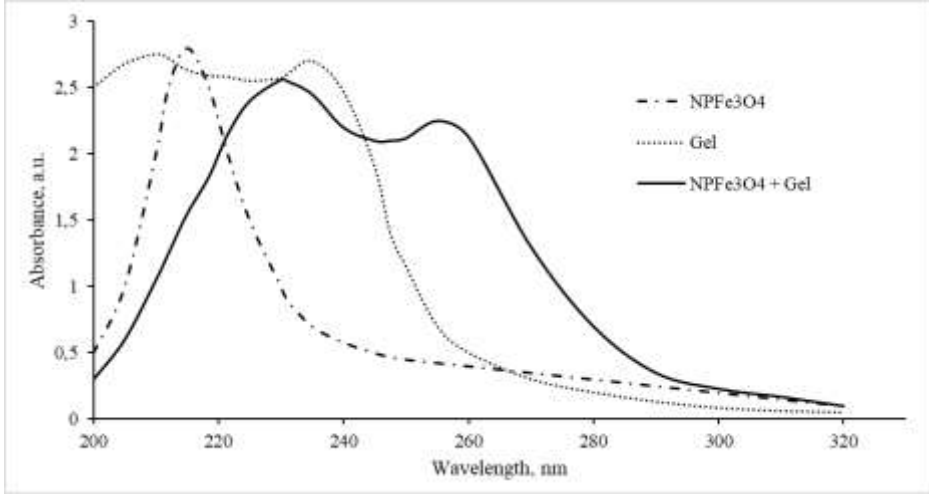

Fig. 5. UV-Vis - Vis - spectra of test samples: – · – $NPFe_3O_4$, ····· – Gel, —— –$NPFe_3O_4$+Gel

In the UV-Vis spectrum of sample 2 – Gel, absorption bands are observed at wavelengths of 210 nm and 235 nm. The first band can be identified as absorption by peptide bonds (the absorption range of which is about 180–230 nm), the second band is due to chromophores of aromatic and heterocyclic amino acid fragments (Gly, Pro, Hyp, *etc*. - the absorption range of which is about 230–240 nm). These spectral fingerprints are the basis for the identification of Gel in complex matrices.[31,35,36] It is also clear from the UV profile of Gel that the absorption of gelatin drops sharply to almost zero above ~235 nm, while after modification of Gel with Fe_3O_4 nanoparticles, an increase in the absorption intensity is observed between 235 nm and 260 nm. A similar effect was observed in Gel-containing nanopolymer compositions.[35]

The UV-Vis spectrum of sample 3 –$NPFe_3O_4$+Gel shows a characteristic surface plasmon resonance (SPR) with absorption bands at wavelengths of 231 nm and 260 nm, detected for Fe_3O_4 nanoparticles modified with gelatin. It is known that the position and shape of surface plasmon bands of metal nanoparticles and their oxides depend to a large extent on such characteristics as the size, shape, and dispersion of the particles. At the same time, these characteristics are strongly influenced by the presence of surfactants (chemical composition, concentration, physicochemical properties, *etc*.). In this context, the smaller and more homogeneous the particles, the narrower the surface plasmon bands will be, and they will tend to be located at lower wavelengths.[35, 52] In the works of Abdullah N.H. *et al.*[53] reported similar results on UV-Vis absorption bands for Fe_3O_4 nanoparticles modified with biopolymers, in particular starch. Based on Mie's theory[54], nanoparticles with different sizes should exhibit different optical properties due to the difference in absorption bands, including the plasmon resonance (SPR) bands. As shown in Fig. 5, the absorption bands of the experimental samples

have different diameters. Therefore, when the particle diameter increased from 70 nm (sample 1 – $NPFe_3O_4$) to 79.4 nm (sample 3 –$NPFe_3O_4$+Gel) (see Table 1), the λ_{max} of the SPR shifted from 215 nm to 260 nm. The absorption peak due to SPR of Gel-modified Fe_3O_4 nanoparticles underwent a red (bathochromic) shift with increasing particle diameter.[55]

3.1.6. Fourier transform infrared spectroscopy

The surface of $NPFe_3O_4$ in an aqueous medium undergoes modification under the influence of OH^--groups, which occurs due to the coordination of H_2O dipoles with unsaturated Fe atoms on the surface of solid Fe_3O_4 nanoparticles. The valence and deformation vibrations of these dipoles are observed at ~3400 cm^{-1} and ~1633 cm^{-1}, respectively.[15,17,55] The intense broad band with an absorption maximum at 3341±4 cm^{-1} in the $NPFe_3O_4$+Gel nanocomplex undergoes a shift to the low-frequency region compared to the vibration frequency of the bonds of free OH^- groups and the amide bond Amide A (N–H), which are observed at 3398±5 and 3408±5 cm^{-1}. A similar effect is observed for the deformation vibrations of the OH^- group. It is worth noting that in the $NPFe_3O_4$+Gel nanocomplex, due to the addition of Fe to the O–H groups, the intensity and width of the band of stretching vibrations of the O–H bond in the region ~ 3400 cm^{-1} decrease. In addition, intense absorption bands with maxima at 2360±4 cm^{-1} and 2342±3 cm^{-1} are observed, which are absent in the spectrum of Gel. These peaks can be attributed to the symmetric stretching (*vs*) vibrations of the C–H bond, which indicates the presence of electrostatic hydrophobic interactions of aliphatic side chains of amino acid residues in nanostructured associates of the "clathrate" and "cavity" type formed under the influence of $NPFe_3O_4$.[6,11] It is known that the vibration frequencies of the amide group of polypeptides, in particular Gel, are located in the range of about 1650, 1540, and 1240 cm^{-1} and are usually designated as Amide I, Amide II and Amide III vibrations, respectively.[56,57] During the adsorption of Gel on the surface of $NPFe_3O_4$, a shift of the absorption bands of the stretching vibrations of Amide I ν(C=O) and the in-plane deformation vibrations of Amide II δ_{pl} is observed. (N–H) towards lower frequencies: ν(C=O) at 1642±3 cm^{-1}, δ_{pl} (N–H) at 1527±3 cm^{-1} respectively.[11,18,32] This indicates an electrostatic interaction between the amide bond and $NPFe_3O_4$. The absorption bands of in-plane and out-of-plane deformation vibrations δ_{pl} (C–H) and δ_{pl} (C–C) are shifted to the lower frequency region: δ_{pl} (C–H) at 1442±3 cm^{-1}, and δ_{pl} (C–C) at 1027±2 cm^{-1}, respectively.

In addition, a new absorption band appears, corresponding to the in-plane deformation vibrations δ_{pl} (C–C) at 1155±2 cm^{-1}. This indicates the presence of electrostatic hydrophobic interactions between aliphatic and alicyclic amino acid residues in the $NPFe_3O_4$+Gel nanocomplex.[8,52]

$NPFe_3O_4$ has characteristic strong peaks between 600 cm^{-1} and 500 cm^{-1}.[18,32] FTIR of sample 1 – $NPFe_3O_4$ showed characteristic peaks at 627 cm^{-1} and 575 cm^{-1}, which correspond to the vibrations of the Fe–O bond. The shift of the maxima of these bands in the $NPFe_3O_4$+Gel nanocomplex to the region of ~ 630 cm^{-1} and ~ 588 cm^{-1} is explained by the influence of Gel molecules, which interact with the surface layer of Fe_3O_4 nanoparticles, penetrate the near-surface region, and chemisorb with Fe^{2+} and Fe^{3+} cations. Therefore, the FTIR results indicate the formation of a structural interaction between Gel and $NPFe_3O_4$.

3.1.7. Thermogravimetric analysis (TGA)

TG analysis showed that in the experimental samples in the temperature range from 50 to 100°C, the first mass loss of all samples occurs, which is associated with the evaporation of physically adsorbed water on the surface of the samples and is accompanied by a mass loss of ~0.7% (sample 1 – $NPFe_3O_4$), ~1.3% (sample 2 – Gel), ~1.0% (sample 3 – $NPFe_3O_4$/Gel). At a temperature of 150°C, for sample 3 – $NPFe_3O_4$/Gel, a decrease in the mass of the sample by 0.8% is observed, which is associated with the desorption of Gel from the surface of $NPFe_3O_4$. When the temperature increases to 200°C, the process of thermal decomposition of Gel begins, which occurs more slowly in the case of $NPFe_3O_4$/Gel, which confirms the chemical interaction of $NPFe_3O_4$ with molecules of the biopolymer – Gel, which contributes to increasing the thermal stability of the $NPFe_3O_4$+Gel nanocomplex. The final decomposition of Gel occurs at 300°C. That is, the TGA method confirms the chemical interaction of $NPFe_3O_4$ with the molecules of the biopolymer – Gel, which contributes to the increase in the thermal stability of the $NPFe_3O_4$+Gel nanocomplex.

3.1.8. Transmission electron microscopy (TEM)

Fig. 6 presents TEM images and histograms showing the particle size distribution for the experimental samples: sample 1 – $NPFe_3O_4$, sample 3 – NP Fe_3O_4+Gel nanocomplex. According to the TEM images (Fig. 6), the morphology, dimensions, and size distribution of particles in experimental samples 1 and 3 were determined. In particular, it was found that sample 1 – $NPFe_3O_4$ (Fig. 7a) is distinguished by the formation of agglomerated clusters of Fe_3O_4 nanoparticles. The shape of Fe_3O_4 nanoparticles is spherical, and the average diameter in the main fraction is <d> 70 nm. Fe_3O_4 nanoparticles are characterized by a

fairly uniform distribution in diameter, close to monodispersity; small sizes, which ensures a high ratio of their surface to volume. Therefore, they have a high surface energy, which provides the ability to sorption and the formation of nanoassociates.

Particles of NP Fe_3O_4+Gel nanoassociates – sample 3 (Fig. 6b) have an almost spherical shape, are monodisperse, and are characterized by an average diameter of the main fraction d~79 nm. Also, the presence of Gel prevents agglomeration of $NPFe_3O_4$, which is due to the chemisorption of Gel on the surface of Fe_3O_4 nanoparticles. This process occurs due to the electrostatic interaction between the dipoles of the amino and carboxy groups of Gel and the diphilic $NPFe_3O_4$, as well as the rotation of gelatin chains around Fe_3O_4 nanoparticles. This prevents coagulation and provides high colloidal stability of the dispersion. The results obtained are consistent with the data presented in studies [15,17,28,35,40].

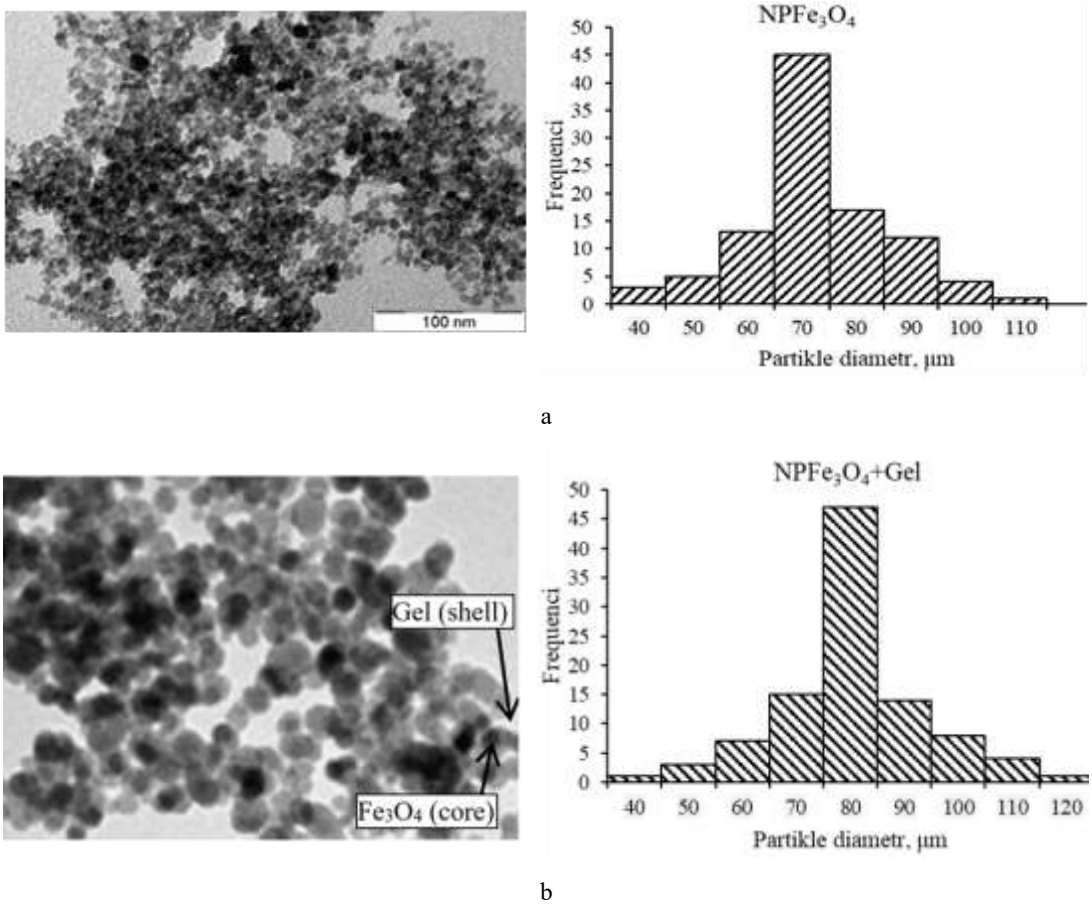

Fig.6. TEM images and histograms showing particle size distribution for test samples: ***a*** – $NPFe_3O_4$, ***b*** – Gel, 3 –$NPFe_3O_4$+Gel

3.2. Substantiation of the mechanism of gelatin binding by Fe_3O_4 nanoparticles in protein-containing systems

3.2.1. Scientific substantiation of the mechanism of binding gelatin with nanoparticles Fe_3O_4

The surface chemical activity of $NPFe_3O_4$ is mainly due to electrostatic interactions, in particular dipole-dipole (Van der Waals) and ion-dipole forces. In the process of protein adsorption on the $NPFe_3O_4$ surface, donor-acceptor (coordination) interactions, such as hydrogen bonds, are also involved.[2,15] Hydrophilic contacts between polar $NPFe_3O_4$ and ionogenic groups of proteins (C–O, C–N, O–H, and S–H) can be formed due to hydrogen bonds caused by electrostatic attraction. This contributes to increasing the stability of the protein+$NPFe_3O_4$ system and slows down the formation of hydrophobic bonds between fragments of biopolymer macromolecules, preventing their aggregation. Therefore, under the action of Fe_3O_4 nanoparticles, protein molecules undergo structural changes in the process of forming complexes with $NPFe_3O_4$, which occurs due to electrostatic interactions.

Fig. 7 shows a complex of Fe_3O_4 nanoparticles with Gel, stabilized by coordination (donor-acceptor) bonds between the iron atoms of $NPFe_3O_4$, oxygen, and nitrogen atoms in the glycine, proline, and hydroxyproline residues (basic amino acids of Gel). Additional stabilization is provided by electrostatic and hydrophobic interactions, in particular in the form of "clusters" of heterocyclic fragments of proline and hydroxyproline residues. As a result, a more branched structure and a more complex interlacing of the protein macromolecule are formed.[2,15]

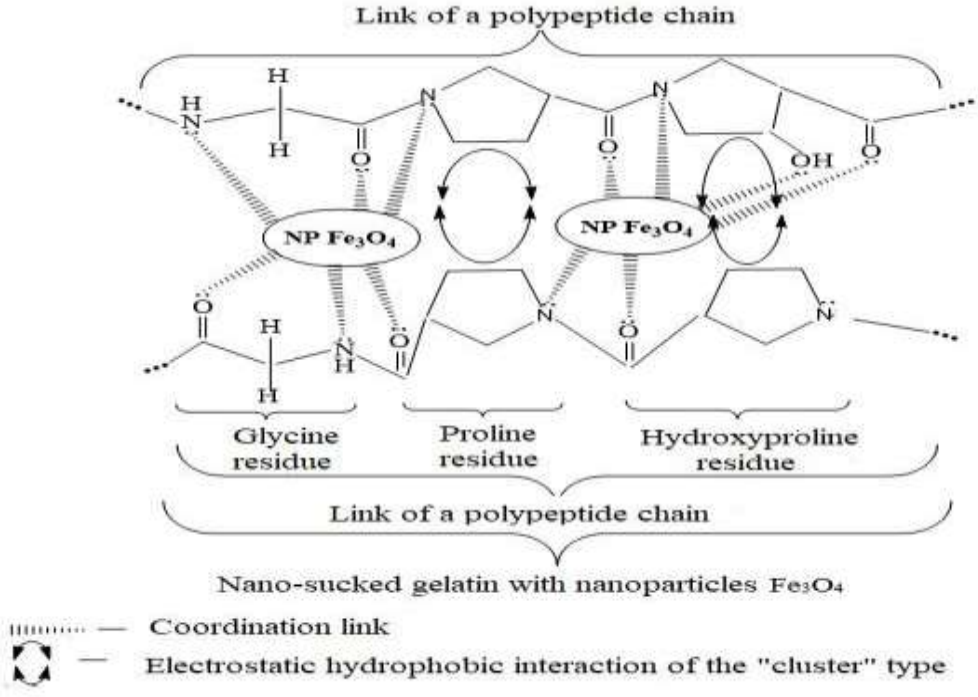

Fig. 7. $NPFe_3O_4$+Gel electrostatic complex

3.2.2. Experimental confirmation of the interaction of Fe_3O_4 nanoparticles with gelatin

In colloidal-dispersed systems, the amphiphilic properties of the components play a crucial role in forming various supramolecular structures, including monolayers, micelles, and liposomes, which contribute to the stability of the dispersions. Fe_3O_4 nanoparticles, in addition to amphiphilicity, are characterized by a large specific surface area, high chemical activity, and the presence of structure-forming cations Fe^{2+} and Fe^{3+}, which determines their ability to form various supramolecular structures. This factor contributes to the stabilization of polyphase systems, as well as the processes of structure formation, foaming, and gelation, which are due to the stabilizing, complexing, and structure-forming properties of $NPFe_3O_4$.[2,3,15,17]

Fe_3O_4 nanoparticles enhance the effect of structure-forming agents, in particular the fibrillar protein Gel, which contributes to an increase in the effective viscosity of gel-containing compositions. The thickening properties of $NPFe_3O_4$ are confirmed by an increase in the viscosity of $NPFe_3O_4$+Gel aqueous solutions depending on the $NPFe_3O_4$ concentration (Fig. 8). The study showed that the addition of Fe_3O_4 nanoparticles to an aqueous solution of gelatin (Gel) causes an increase in viscosity in the entire range of shear stress (γ=1.5–40 s^{-1}) by 1.22–1.27 times compared to the control sample (Fig. 8a). This is explained by the presence of structure-forming cations Fe^{2+} and Fe^{3+} on the surface of Fe_3O_4, as well as the electrostatic interaction of $NPFe_3O_4$ with Gel macromolecules. As a result, a three-dimensional network formed by Gel hydrocolloid molecules is formed, which is stabilized by $NPFe_3O_4$.[17,57]

The study confirmed the thixotropic properties of $NPFe_3O_4$+Gel gel-like systems (Fig. 8 b). In particular, the addition of Fe_3O_4 nanoparticles to the Gel solution contributes to an increase in the thixotropy coefficient (K_{thix}) by 1.3–1.5 times. The addition of $NPFe_3O_4$ to the aqueous Gel solution slows down the destruction of the gel-like structure by 1.14–1.23 times and accelerates its recovery after the cessation of mechanical action by 8.7–9.1%. Additionally, it increases the thixotropic properties by an average of 1.40±0.5 times. This effect is due to the surface-active properties of $NPFe_3O_4$ and their ability to

form a certain consistency, stabilizing the dispersed system and preventing its delamination.[17,57]

The optimal concentration of $NPFe_3O_4$ is 1.5% by weight of the colloidal-dispersed solution, since a further increase in the content of nanoparticles has almost no effect on the change in the rheological properties, in particular the viscosity, of the gel-like solution. The study showed that the strength of the gel-like jelly $NPFe_3O_4$+Gel (sample 3) increases by 1.35–1.61 times compared to the control sample (sample 1) when $NPFe_3O_4$ is added with a concentration of 1.5% by weight of the colloidal solution (Fig. 9).

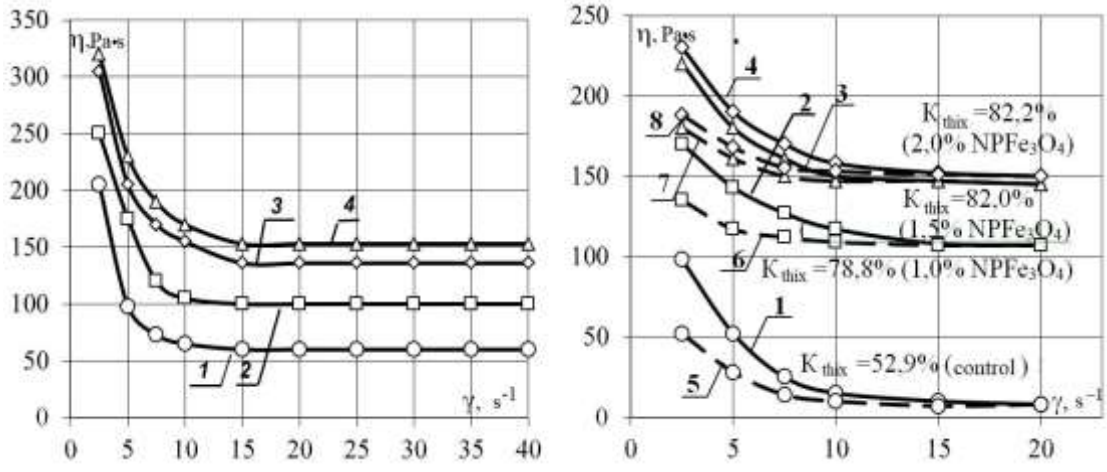

a b

Fig. 8. Dependence of effective viscosity (a) and thixotropic recovery (b) of experimental samples of $NPFe_3O_4$+Gel gel-like systems on $NPFe_3O_4$ concentration, %: 1 – 0-control; 2 – 1,0; 3 – 1,5; and 4 – 2,0 (forward motion); 5 – 0-control; 6 – 1,0; 7 – 1,5; and 8 – 2,0 (reverse motion)

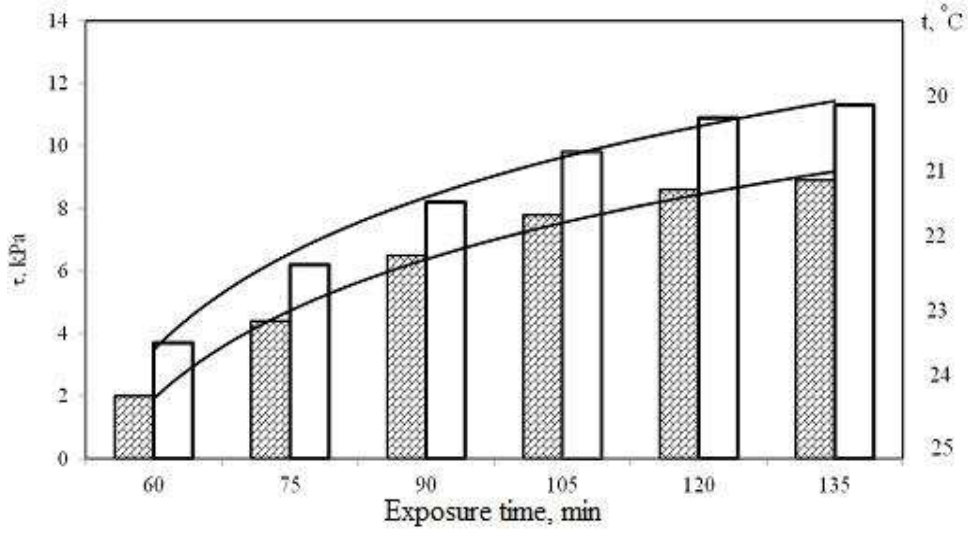

Fig. 9. Dependence of the shear stress limit of $NPFe_3O_4$+Gel gel-like systems on the duration of exposure at different temperatures: (1 – control; 2 – sample with 1.5% $NPFe_3O_4$)

That is, the study of the structural and mechanical properties of $NPFe_3O_4$+Gel gel-like systems confirms that Fe_3O_4 nanoparticles contribute to the stabilization of their polyphase structure. The use of $NPFe_3O_4$ allows you to reduce the content of the structure-forming agent-Gel by 8.0–10.0%, while simultaneously accelerating and enhancing the processes of structure formation.

Thus, it has been experimentally proven that $NPFe_3O_4$ exhibits thickening, thixotropic, and stabilizing properties, as well as the ability to chemically interact and structure formation with Gel molecules.

4. Conclusions

1. The mechanism of interaction of Fe_3O_4 nanoparticles with Gel is substantiated:

– it was established that $NPFe_3O_4$ can self-organize into electrostatic complexes with Gel due to the formation of hydrogen bonds, van der Waals forces, and electrostatic coordination interactions;

– it was found that in polyphase systems containing proteins (Gel), H_2O, and other components, the structure-forming, gel-forming, and stabilizing properties of $NPFe_3O_4$ are regulated due to their amphiphilicity, clusterophilicity, as well as the ability of iron oxide nanoparticles to polarization, electrostatically coordinate, and form supramolecular structures.

2. The mechanism of interaction of Fe_3O_4 nanoparticles with the fibrillar protein Gel was experimentally confirmed:

– using IR-Fourier spectroscopy, it was established that there is an interaction between the functional groups of Gel and $NPFe_3O_4$, which is manifested in the appearance of new absorption bands and the shift of some characteristic bands to the lower frequency region;

– using UV-Vis spectroscopy, chemisorption of Gel on the surface of Fe_3O_4 nanoparticles was confirmed – the absorption peak, due to the surface plasmon resonance (SPR) of Fe_3O_4 nanoparticles modified by Gel, underwent a bathochromic shift – from 215 nm to 260 nm (compared to $NPFe_3O_4$) with an increase in the diameter of the nanoassociate particles;

– a study using the dynamic light scattering method showed that the ζ-potential of the $NPFe_3O_4$+Gel dispersed system increases by 1.12–1.14 times compared to $NPFe_3O_4$ and by 2.14–2.16 times compared to Gel. At the same time, the ζ-potential of the $NPFe_3O_4$+Gel system reaches quite high values 33.0–34.0 mV, which provides the possibility of stabilizing dispersed systems based on proteins by Fe_3O_4 nanoparticles. An increase in the hydrodynamic particle size compared to the nominal value (<d>70 nm) was established: for $NPFe_3O_4$ in aqueous solution – to 77.8–78.8 nm, which is due to the presence of H_2O molecules on their surface. In addition, as a result of chemisorption of Gel, the particle size in the $NPFe_3O_4$+Gel nanocomplex increases to 116.6–117.8 nm;

– the chemical composition of the surface of Fe_3O_4 nanoparticles modified with amino acids: glycine (Gly), proline (Pro), and hydroxyproline (Hyp) was studied by X-ray photoelectron spectroscopy. The XP-spectral profiles of O (1s) of the experimental samples $NPFe_3O_4$, $NPFe_3O_4$+Gly, $NPFe_3O_4$+Pro, and $NPFe_3O_4$+Hyp have peaks at 529.5, 531.0, 533.4, and 533.9 eV, respectively, and are due to O–H/Fe–O bonds, which indicate the chemical interaction of $NPFe_3O_4$ with amino acids. The C (1s) peaks in nanoassociates: $NPFe_3O_4$+Gly at 284.2 and 288.4 eV are due to σ(C–H)/σ(C–N) and π (O–C=O) bonds, respectively; $NPFe_3O_4$+Pro at 288.8 and 292.6 eV and $NPFe_3O_4$+Hyp at 290.6 and 294.4 eV are due to the bonds σ(C–H)/π(O–C=O) and σ(C–N), respectively. A slight shift of the peaks towards higher energy, both in Pro and Hyp, and in their nanoassociates with $NPFe_3O_4$, is associated with electrostatic, steric, and other interactions of Fe_3O_4 nanoparticles with biomolecules. This is a confirmation of the chemisorption of amino acids on the surface of Fe_3O_4 nanoparticles:

– the elemental composition of $NPFe_3O_4$, Gel and $NPFe_3O_4$+Gel samples was investigated by energy-dispersive X-ray spectroscopy. The obtained results confirmed the process of adsorption and chemical interaction of Fe_3O_4 nanoparticles with Gel;

– X-ray diffraction (XRD) studies confirmed the crystalline structure of the experimental nanoparticle samples and an increase in the size of the crystallites of the $NPFe_3O_4$+Gel nanocomplex to 79.44 nm compared to 70.04 nm ($NPFe_3O_4$);

– analysis of TEM images established an almost spherical morphology of practically monodisperse nanoparticles: $NPFe_3O_4$ and $NPFe_3O_4$+Gel with an average size of 67–73 and 77–81 nm, respectively. At the same time, the presence of Gel prevents agglomeration of $NPFe_3O_4$, which is due to chemisorption of Gel on the surface of Fe_3O_4 nanoparticles;

– thermogravimetric analysis determined a decrease in weight loss at the second 100–150°C and third 150–200°C stages in the $NPFe_3O_4$+Gel nanocomplex (compared to $NPFe_3O_4$ and Gel), which confirms the chemical interaction of $NPFe_3O_4$ with the molecules of the biopolymer – Gel and contributes to increasing the thermal stability of the $NPFe_3O_4$+Gel nanocomplex;

– structural and mechanical studies have proven the structure-forming and stabilizing properties of Fe_3O_4 nanoparticles – an increase in the effective viscosity of the $NPFe_3O_4$+Gel gel-like systems by 1.22–1.27 times, an increase in the thixotropy coefficient (K_{thix}) by 1.3–1.5 times and an increase in the strength of the gel-like gel by 1.35–1.61 times with an increase in the $NPFe_3O_4$ concentration from 1.0 to 2.0% by weight of the solution was established.

The results obtained will contribute to the modeling of structure-forming processes (gelation, foaming, *etc*.) in various technological environments, stabilization of multiphase systems, as well as optimization of functional and technological properties of protein-containing compositions, and improvement of the quality indicators of finished products. It is worth noting that of practical interest is the study of the processes of chemisorption of various biopolymers (proteins of multiple origins, lipids,

carbohydrates, *etc*.) on the surface of Fe_3O_4 nanoparticles, as well as the mechanisms of microstructure formation of polyphase systems with the addition of $NPFe_3O_4$, in particular gelation, foaming, and dispersion stabilization.

References

[1] Chavali1, M.S.; Nikolova. M.P. Metal Oxide Nanoparticles and Their Applications in Nanotechnology. *SN Applied Sciences* **2019**, *1*, 607. https://doi.org/10.1007/s42452-019-0592-3

[2] Tsykhanovska, I.; Evlash, V.; Oleksandrov, O.; Gontar, T. Mechanism of Fat-Binding and Fat-Contenting of the Nanoparticles of a Food Supplement on the Basis of Double Oxide of Two- and Trivalent Iron. *Ukr. Food J.* **2018**, *7*, 702–715. https://doi.org/10.24263/2304-974X-2018-7-4-14

[3] Drmota, A.; Kosak, A.; Znidarsik A. A Mechanism for the Adsorption of Carboxylic Acids onto the Surface of Magnetic Nanoparticles. *Materials and technology* **2008**, *42*, 79–83.

[4] Li, J.; Pylypchuk, I.; Johansson, D.; Kessler, V.; Seisenbaeva, G. Self-Assembly of Plant Protein Fibrils Interacting with Superparamagnetic Iron Oxide Nanoparticles. *Sci. Rep.* **2019**, *9*, 8939. https://doi.org/10.1038/s41598-019-45437-z

[5] Tsykhanovska, I.; Evlash, V.; Alexandrov, A.; Lazarieva, T.; Svidlo, K.; Gontar, T.; Yurchenko, L.; Pavlotska, L. Substantiation of the Mechanism of Interaction between Biopolymers of Rye-and-wheat Flour and the Nanoparticles of the Magnetofood. Food Additive in Order to Improve Moisture-retaining Capacity of Dough. *East.-Eur. J. Enterp. Technol.* **2018**, *2/11 (92)*, 70–80. https://doi.org/10.15587/1729-4061.2018.126358

[6] Dickinson, E. Stabilising Emulsion-Based Colloidal Structures with Mixed Food Ingredients. *J. Sci. Food Agric.* **2013**, *93*, 710–721. https://doi.org/10.1002/jsfa.6013

[7] Goralchuk, A.; Gubsky, S.; Omelchenko, S.; Riabets, O.; Grinchenko, O.; Fedak, N.; Kotlyar, O.; Cheremska, T.; Skrynnik, V. Impact of Added Food Ingredients on Foaming and Texture of the Whipped Toppings: A Chemometric Analysis. *Eur. Food Res. Technol.* **2020**, *246*, 1955–1970. https://doi.org/10.1007/s00217-020-03547-3

[8] Harper, W.J.; Hewitt, S.A.; Huffman, L.M. Model Food Systems and Protein Functionality. In Milk Proteins: From Expression to Food; Academic Press: Cambridge, MA, USA, 2019; pp. 573–598. https://doi.org/10.1016/B978-0-12-815251-5.00015-3

[9] Sanguansri, P.; Augustin, M.A. Nanoscale Materials Development—A Food Industry Perspective. *Trends Food Sci. Technol.* **2006**, *17*, 547–556. https://doi.org/10.1016/j.tifs.2006.04.010

[10] Tsykhanovska, I.; Stabnikova, O.; Gubsky, S. Spectroscopic Studies of Interaction of Iron Oxide Nanoparticles with Ovalbumin Molecules. *Mater. Proc.* **2022**, *9*, 1–8. https://doi.org/10.3390/materproc2022009002

[11] Mikhailov, O.V. Gelatin as It Is: History and Modernity. *Int. J. Mol. Sci.* **2023**, *24*, 3583. https://doi.org/10.3390/ijms24043583

[12] Thiruvengadam, M.; Rajakumar G.; Chung M. Nanotechnology: Current Uses and Future Applications in the Food Industry. *3 Biotech*. **2018**, *8*, 74. https://doi.org/10.1007/s13205-018-1104-7

[13] Hansen, S. F.; Heggelund, L. R.; Besora, P. R.; Mackevica, A.; Boldrin, A.; Baun, A. Nanoproducts–what is Actually Available to European consumers? *Environ. Sci.: Nano*. **2016**, *3*, 169–180. https://doi.org/10.1039/C5EN00182J

[14] Ramachandraiah, K.; Choi, M.; Hong G. Micro- and Nano-Scaled Materials for Strategy-Based Applications in Innovative Livestock Products: A Review. *Trends Food Sci. Technol*. **2018**, *71*, 25–35. https://doi.org/10.1016/j.tifs.2017.10.017

[15] Tsykhanovska, I.; Riabchykov, M.; Alexandrov, O.; Evlash, V.; Bryzytska, O.; Gubsky, S.; Lazareva, T.; Blahyi, O. Hysico-Chemical Studies of the Interaction Mechanism of Double and Trivalent Iron Double Oxide Nano-Particles with Serpin Protein Ovalbumin and Water. *Chem. Chem. Technol.* **2023**, *17*, 481–494. https://doi.org/10.23939/chcht17.03.481

[16] Tsykhanovska, I.; Evlash, V.; Alexandrov, A.; Gontar, T. Dissolution Kinetics of Fe_3O_4 Nanoparticles in the Acid Media. *Chem. Chem. Technol.* **2019**, *13*, 170–184. https://doi.org/10.23939/chcht13.02.170

[17] Tsykhanovska, I.; Evlash, V.; Alexandrov, A.; Gontar, T.; Shmatkov, D. The study of the interaction mechanism of linoleic acid and 1-linoleyl-2-oleoyl-3-linolenoyl-glycerol with Fe_3O_4 nanoparticles. *Chem. Chem. Technol.* **2019**, *13*, 303–316. https://doi.org/10.23939/chcht13.03.303

[18] Yılmaz, H.; Sanlıer, S.H. Preparation of Magnetic Gelatin Nanoparticles and Investigating the Possible Use as Chemotherapeutic Agent. *Artif. Cells Nanomed. Biotechnol*. **2013**, *41*, 69–77. https://doi.org/10.3109/21691401.2012.745863

[19] Stevens, J. S.; De Luca, A. C.; Pelendritis, M. Quantitative Analysis of Complex Amino Acids and RGD Peptides by X-ray Photoelectron Spectroscopy (XPS). *Surf. Interface Anal.* **2013,** *45*, 1238–1246. https://doi.org/10.1002/sia.5261

[20] Meyer, F.; Hauschild, D.; Benkert, A.; Blum, M.; Yang, W.; Reinert, F.; Heske, C.; Zharnikov, M.; Weinhardt, L. Resonant Inelastic Soft X-ray Scattering and X-ray Emission Spectroscopy of Solid Proline and Proline Solutions. *J. Phys. Chem. B.* **2022**, *126*, 10185–10193. https://doi.org/10.1021/acs.jpcb.2c06557

[21] Stevie, F. A.; Donley, C. L. Introduction to X-ray Photoelectron Spectroscopy. *J. Vac. Sci. Technol.* **2020**, A *38*, 063204. https://doi.org/10.1116/6.0000412

[22] Baer, D.R. Guide to Making XPS Measurements on Nanoparticles. *J. Vac. Sci. Technol.* **2020**, *A 38*, 031201. https://doi.org/10.1116/1.5141419

[23] Maity, D.; Kale, S. N.; Kaul-Ghanekar, R.; Xue, Jun-Min; Ding, J. Studies of Magnetite Nanoparticles Synthesized by Thermal Decomposition Ofiron (III) Acetylacetonate in tri(Ethylene glycol). *J. Magn. Magn. Mater.* **2009**, *321*, 3093–3098. https://doi.org/10.1016/j.jmmm.2009.05.020

[24] Kaznacheyev, K.; Osanna, A.; Jacobsen, C.; Plashkevych, O.; Vahtras, O.; Carravetta, V.; Hitchcock, A. P. Innershell Absorption Spectroscopy of Amino Acids. *J. Phys. Chem. A.* **2002**, *106*, 3153–3168. https://doi.org/10.1021/jp013385w

[25] Xiaoxue, Z.; Hao, W.; Anping, H.; Haiyan, X.; Yongcai, Z.; Dunbo, Yu.; Bo, W.; Hui, Ya. Synthesis of Cadmium Titanate Powders by a Sol-Gel-Hydrothermal Method. *J. Mat. Sci.* **2003**, *38*, 2353–2356. https://doi.org/10.1023/A:1023932513481

[26] Cornell, R. M.; Schertmann, U. *The iron oxides: structure, properties, reactions, occurrence and uses*; VCH Publishers: Weinheim, 2000; pp 142–278.

[27] Gaihre, B.; Aryal, S.; Barakat, N.A.M.; Kim, H.Y. Gelatin Stabilized Iron Oxide Nanoparticles as a Three Dimensional Template for the Hydroxyapatite Crystal Nucleation and Growth. *Mater. Sci. Eng. C* **2008**, *28*, 1297–1303. https://doi.org/10.1016/j.msec.2008.01.001

[28] Ulfa, M.; Poetry, S. D. Gelatin's Effect on Iron Oxide Nanoparticle Properties and Its Use in Thermal Regeneration for Methylene Blue Photodegradation. *Bull. Chem. React. Eng. Catal.* **2024**, *19*, 384–392. https://doi.org/10.9767/bcrec.20172
[29] Ulfa, M.; Anggreani, C. N.; Sholeha, N. A. Fine-Tuning Mesoporous Silica Properties by a Dual-Template Ratio as TiO_2 Support for Dye Photodegradation Booster. *Heliyon* **2023**, *9*, e16275. https://doi.org/10.1016/j.heliyon.2023.e16275
[30] Babu, T. S. R.; Neeraja, D. A Experimental Study of Natural Admixture Effect on Conventional Concrete and High Volume Class F Flyash Blended Concrete. *Case Studies in Construction Materials* **2017**, *6*, 43–62. https://doi.org/10.1016/j.cscm.2016.09.003
[31] Farya, K.; Waheed, U.; Ahmad, K. S.; Noor, A. U.; Mujtab, H. S.; Hikmat, U.; Nawab, A.; Iqbal, M. Using Gelatin-Iron Oxide Nanoplexes as binder and Preservative for Minced Beef Meat. *Journal of Xi'an Shiyou University, Natural Science Edition* **2023**, *19*, 384–391. http://xisdxjxsu.asia
[32] Parkatzidis, K.; Kabouraki, E.; Selimis, A.; Kaliva, M.; Ranella, A.; Farsari, M.; Vamvakaki, M. Initiator-Free, Multiphoton Polymerization of Gelatin Methacrylamide. *Macromol. Mater. Eng.* **2018**, *303*, 1800458. https://doi.org/10.1002/mame.201800458
[33] Astuti, A.I.; Soejoedono, R. D.; Saepudin, E.; Assaat, L. D.; Ivandini, T. A. Polyclonal Antibodies Production from Porcine Gelatin and its Preliminary Study for Immunosensor Applications. *IOP Conf. Ser.: Mater. Sci. Eng*. **2020**, *763*, 012007. https://doi.org/10.1088/1757-899X/763/1/012007
[34] Aminu, M.; Mansor, B. A.; Mohd Zobir, H.; Mohd Izham, S.; Abubakar, S. H. Effect of Gelatin-Stabilized Copper Nanoparticles on Catalytic Reduction of Methylene Blue. *Nanoscale Res. Lett.* **2016**, *11*, 438–454. https://doi.org/10.1186/s11671-016-1656-6
[35] Aguilar-Méndez, M.A.; Espinosa-Solares, T.; Guerrero-Toledo, F. M.; Canseco-González, D.; Velázquez-Hernández, A.; Aguilar-Moreno, G. S.; Navarro-Cerónnava, E. Synthesis And Characterisation Of Magnetite Nanoparticles Using Gelatin and Starch as Capping Agents. *IET Nanobiotechnol*. **2020**, *14*, 94–97. https://doi.org/10.1049/iet-nbt.2019.0204
[36] Dantas, M.; Tenório, H.; Lopes, T.; Pereira, H.; Marsaioli, A.; Figueiredo, I.; Santos, J. Interactions of Tetracyclines with Ovalbumin, the Main Allergen Protein from Egg White: Spectroscopic and Electrophoretic Studies. *Int. J. Biol. Macromol*. **2017**, *102*, 505–514. https://doi.org/10.1016/j.ijbiomac.2017.04.052
[37] Saragi, T.; Santika, A. S.; Permana, B.; Syakir, N.; Kartawidjaja, M.; Risdiana, R. Synthesis and Properties of Iron Oxide Particles Prepared by Hidrothermal Method. *IOP Conf. Ser.: Mater. Sci. Eng*. **2017,** *196*, 012025. https://doi.org/10.1088/1757-899X/196/1/012025
[38] Takai, Z. I.; Mustafa, M. K.; Asman, S.; Sekak, K. A. Preparation and Characterization of Magnetite (Fe_3O_4) nanoparticles By Sol-Gel Method. *Int. J. Nanoelectron. Mater.* **2019**, *12*, 37–46. https://doi.org/10.11113/mjfas.v15n2019.1224
[39] Ghalenavi, H.; Hemmati-Sarapardeh, A.; Schaffie, M.; Norouzi-Apourvari, S. Application of Synthesized Fe_3O_4@Gelatin Nanoparticles on Interfacial Properties and Enhanced Oil Recovery. *Sci. Rep.* **2025**, *15*, 2558. https://doi.org/10.1038/s41598-024-84953-5
[40] Dung, T.T.; Danh, T. M.; Hoa, L. T. M.; Chien, D. M.; Duc, N. H. Structural and Magnetic Properties of Starch-Coated Magnetite Nanoparticles. *J. Exp. Nanosci.* **2009**, *4*, 259–267. https://doi.org/10.1080/17458080802570609
[41] Iglesias-Silva, E.; Rivas, J.; León Isidro, L.M.; López-Quintela, M.A. Synthesis of Silver-Coated Magnetite Nanoparticles. *J. Non-Cryst. Solids* **2007**, *353*, 829–831. https://doi.org/10.1016/j.jnoncrysol.2006.12.050
[42] Ottone, M.L.; Peirotti, M. B.; Deiber, J. A. Rheokinetic Model to Characterize the Maturation Process of Gelatin Solutions under Shear Flow. *Food Hydrocolloids* **2009**, *23*, 1342–1350. https://doi.org/10.1016/j.foodhyd.2008.11.011
[43] Casas-Forero, N.; Orellana-Palma, P.; Petzold, G. Comparative Study of the Structural Properties, Color, Bioactive Compounds Content and Antioxidant Capacity of Aerated Gelatin Gels Enriched with Cryoconcentrated Blueberry Juice during Storage. *Polymers* **2020**, *12*, 2769. https://doi.org/10.3390/polym12122769
[44] Pawar, N.; Bohidara, H. B. Surface Selective Binding of Nanoclay Particles to Polyampholyte Protein Chains. *J. Chem. Phys.* **2009**, *131*, 045103. https://doi.org/10.1063/1.3184803
[45] Sankhla, A.; Sharma, R.; Yadav, R. S.; Kashyap, D.; Kothari, S. L.; Kachhwaha S. Biosynthesis and Characterization of Cadmium Sulfide Nanoparticles – An Emphasis of Zeta Potential Behavior Due to Capping. *Mater. Chem. Phys*. **2016**, *170*, 44–51. https://doi.org/10.1016/j.matchemphys.2015.12.017
[46] Atefeh, S. Y.; Shiva, A. B.; Nasser, N. Porous Scaffolds with the Structure of an Interpenetrating Polymer Network Made by Gelatin Methacrylated Nanoparticle-Stabilized High Internal Phase Emulsion Polymerization Targeted for Tissue Engineering. *RSC Adv*. **2021**, *11*, 22544–22555. https://doi.org/10.1039/d1ra03333f.
[47] Masuelli, M. A.; Sansone, M. G. Hydrodynamic properties of Gelatine. Studies from intrinsic viscosity measurements. Chapter 5. Book: Products and Applications of Biopolymers; Verbeek, C. J. R., Ed.; INTECH: Croatia, 2012; pp 85–116. https://doi.org/10.5772/34401
[48] Papachrisanthou, K. The Effect of Gelatin pH and Incubation Time on the Size of Nanoparticles Manufactured by Desolvation. *Honors Theses* **2022**, 2566. https://egrove.olemiss.edu/hon_thesis/2566
[49] Azcona, P.; Zysler, R.; Lassalle, V. Simple and Novel Strategies to Achieve Shape and Size Control of Magnetite Nanoparticles Intended for Biomedical Applications. *Colloids Surf. A.* **2016**, *504*, 320–330. https://doi.org/10.1016/j.colsurfa.2016.05.064
[50] Maestro, A.; Santini, E.; Zabiegaj, D.; Llamas, S.; Ravera, F.; Liggieri, L.; Ortega, F.; Rubio, R.G.; Guzman E. Particle and Particle-Surfactant Mixtures at Fluid Interfaces: Assembly, Morphology, and Rheological Description. *Adv. Condens. Matter Phys.* **2015**, *17*, 917516. https://doi.org/10.1155/2015/917516
[51] Dzwolak, W.; Kato, M.; Taniguchi, Yo. Fourier Transform Infrared Spectroscopy in High-Pressure Studies on Proteins. *Biochim. Biophys. Acta - Protein Structure and Molecular Enzymology* **2002**, 1595, 131–144. https://doi.org/10.1016/S0167-4838(01)00340-5
[52] Klekotka, U.; Satuła. D.; Spassov S. Surfactant Dependence on Physicochemical Properties of Magnetite Nanoparticles. *Colloid. Surf. A*. **2018**, *537*, 452–459. https://doi.org/10.1016/j.colsurfa.2017.10.054
[53] Abdullah, N.H.; Shameli, K.; Abdullah, E.C. A Facile and Green Synthetic Approach Toward Fabrication of Starch-Stabilized Magnetite Nanoparticles. *Chinese Chem. Lett*. **2017**, *28*, 1590–1596. https://doi.org/10.1016/j.cclet.2017.02.015

[54] Majid, D.; Mansor, A.B.; Khorsand, Z.A.; Reza, Z.; Mohammad H. Fabrication and Characterization of Gelatin Stabilized Silver Nanoparticles under UV-Light. *Int. J. Mol. Sci*. **2011**, *12*, 6346–6356. https://doi.org/10.3390/ijms12096346
[55] Byler, D.M.; Susi, H. Examination of the Secondary Structure of Proteins by Deconvolved FTIR Spectra. *Biopolymers* **1986**, *25*, 469–487. https://doi.org/10.1002/bip.360250307
[56] Tsykhanovska, I.; Evlash, V.; Blahyi, O. Mechanism of Water-Binding and Water-Retention of Food Additives Nanoparticles Based on Double Oxide of Two- and Trivalent Iron. *Ukr. Food J*. **2020**, *9*, 298–321. https://doi.org/10.24263/2304-974x-2020-9-2-4
[57] Tsykhanovska, I.; Evlash, V.; Alexandrov, O.; Riabchykov, M.; Lazarieva, T.; Nikulina A., Blahyi O. Chapter 1. Technology of Bakery Products Using Magnetofood as a Food Additive. In *Bioenhancement and Fortification of Foods for a Healthy Diet*; Paredes-López, O.; Shevchenko, O.; Stabnikov, V.; Ivanov, V., Eds; Boca Raton, 2022, pp 1–45. https://doi.org/10.1201/9781003225287

Received: May 12, 2025 / Revised: June 20, 2025 / Accepted: June 24, 2025

ФІЗИКО-ХІМІЧНІ ДОСЛІДЖЕННЯ МЕХАНІЗМУ ВЗАЄМОДІЇ НАНОЧАСТИНОК ПОДВІЙНОГО ОКСИДУ ДВО- ТА ТРИВАЛЕНТНОГО ФЕРУМУ З ФІБРИЛЯРНИМ БІЛКОМ-ЖЕЛАТИНОМ

Анотація. *У роботі досліджено механізм взаємодії наночастинок подвійного оксиду феруму (Fe_3O_4) з фібрилярним білком желатином (Gel) за допомогою комплексу фізико-хімічних методів. Уперше встановлено, що утворення стабільного міжмолекулярного комплексу обумовлено амфіфільними та кластерофільними властивостями наночастинок Fe_3O_4, їхньою здатністю до поляризації, електростатичної взаємодії й утворення надмолекулярних структур. Поглинання в ділянці 260 нм (UV-Vis спектроскопія) свідчить про формування плазмонного резонансу в системі NPFe_3O_4/Gel. Динамічне розсіювання світла (DLS) показало середній гідродинамічний діаметр частинок ~79,0 нм, що узгоджується з даними рентгеноструктурного аналізу (XRD) і підтверджує хемосорбцію білка-Gel на поверхні наночастинок Fe_3O_4. Робота має наукову новизну щодо розуміння специфіки зв'язування біополімерів з наноструктурами оксидів металів.*

Ключові слова: *Fe_3O_4, наночастинки, Gel, хемосорбція, нано-асоціати.*